Journal of Engineering Physics and Thermophysics, Vol. 71, No. 2, 1998

A STUDY OF MACROLIQUATION IN SOLIDIFICATION OF A THIN STRIP OF A BINARY MIXTURE PRODUCED BY CONTINUOUS CASTING

A. V. Kuznetsov

UDC 536.242

This is a study of the trends in macroliquation of an impurity in continuous casting of a thin strip produced of a binary mixture. Special attention is paid to analysis of the effect of forced convection, interdendrite filtration, diffusion, and the rate of drawing on redistribution of the impurity.

Different aspects of heat transfer and flow of liquid metal that arise in continuous casting of thin strips have been studied rather recently in [1-3]. The main goal of the present study is analysis of macroliquation in continuous casting of thin-strip products of a binary alloy. To achieve this goal, we suggest a mathematical model that describes the combined processes of heat transfer, flow of the melt, and impurity transfer that determine the process being studied. A numerical solution of equations that constitute the obtained mathematical model is presented.

In the last decade, much of the attention of researchers in heat and mass transfer has been devoted to the development of complicated mathematical models that are able to describe adequately and to predict the complicated thermophysical processes that take place in solidification of binary and multicomponent alloys. Derivation of a system of differential equations for a two-phase region which is based on the approach of the theory of mixtures was presented initially in [4, 5]. Recently, that model has been extended to microlevel processes and presented in [6, 7]. The derivation of a similar system of differential equations based on the averaging method is described in [8-10]. An excellent review of various models with a description of each of them is given in [11]. A new model of the two-phase region that includes the presence of solid, liquid, and gaseous phases is suggested in [12]. Since the time of publication of these works, processes that occur in solidification of binary alloys have been actively simulated with supercomputers. Results of such numerical simulation and characteristic features of the numerical procedures used are presented in [13-26].

Unlike the previous studies, the process considered in the present article is characterized by strong forced convection of liquid metal that is brought about by changes in the height of the free surface. We proceed from the system of differential equations that was obtained with the averaging method and described in [8, 9, 15]. That system of differential equations is modified to include specificity of the casting process studied. It is necessary to modify the system of differential equations because the models mentioned above are poorly suited for simulation of solidification with strong forced convection. In [13-26], the case of rather weak natural convection is mainly considered.

Mathematical Model. The scheme of the process considered in the present article is shown in Fig. 1. A liquid melt flow is supplied to a casting table subjected to high-intensity cooling. The metal flow over the table is described as the flow of a solidifying liquid which has a free surface. At the end of the casting table the solidified strip is drawn at a constant rate U. Special procedures are used to eliminate almost completely friction between the solidified crust in the bottom of the layer and the casting table.

It is assumed that the melted material gets to the casting table at a temperature slightly exceeding the initial solidification temperature and that the distribution of the velocity of the liquid metal entering the casting table is parabolic and corresponds to the steady-state flow. In writing the conservation equations, it is assumed that the present process is described with sufficient accuracy by a two-dimensional and steady-state model and

Technical University of Vienna, Austria. Translated from Inzhenerno-Fizicheskii Zhurnal, Vol. 71, No. 2, pp. 254-262, March-April, 1998. Original article submitted November 11, 1996.

 1062-0125/98/7102-0254$20.00

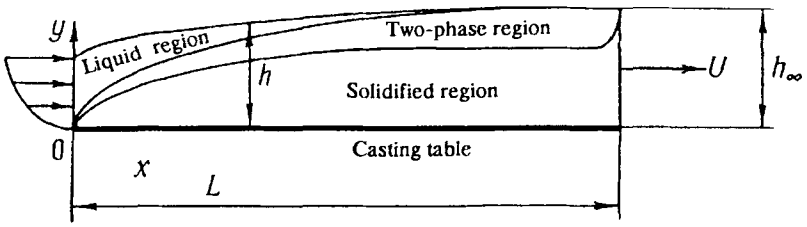

Fig. 1. Scheme of the process.

that the thin-layer approximation is applicable here. The latter fact allows us to make the differential equations that describe the present problem parabolic. It is assumed that liquid and solid phases are isotropic, thermophysical properties of the phases are constant, and deformation and relative motion in the solid phase and formation of gas porosity in the two-phase region can be neglected. Nevertheless, thermophysical properties of the solid and liquid phases can be different.

As regards the diffusion mechanism of impurity transfer, it is assumed that diffusion of the impurity in the solid phase can be neglected on the macrolevel. Nevertheless, on the microlevel (inside the control volume on which averaging is performed), it is assumed that the impurity distribution is equilibrium in the solid phase. This assumption is extremely popular in modeling of macroliquation in binary alloys and is used in almost all the publications mentioned above. To a great extent, this can be explained by the substantial simplification introduced to the mathematical model by this assumption. Indeed, without this assumption, it would be necessary to take into consideration the "history" of the impurity distribution on the microlevel, which would result in an integro-differential system of equations.

In modeling of the free surface, it is assumed that the radiative and convective heat transfer from the free surface is negligible and surface tension can be neglected on the free surface.

With the aforesaid assumptions, the system of differential equations suggested in [8, 9, 15] becomes parabolic and is written in the following dimensionless form.

The momentum equation

$$\varepsilon \frac{\partial \bar{u}}{\partial \bar{x}} + \left[\bar{u}\frac{\partial \bar{u}}{\partial \bar{x}} + \bar{v}\frac{\partial \bar{u}}{\partial \bar{y}}\right] = -\varepsilon^2 \frac{d\bar{p}}{\partial \bar{x}} + \frac{\varepsilon}{\delta^2 \mathrm{Re}}\frac{\partial^2 \bar{u}}{\partial \bar{y}^2} - \varepsilon^2\left(\frac{1}{\mathrm{ReDa}} + \frac{F}{\mathrm{Da}^{1/2}}|\bar{u}|\right)\bar{u}. \tag{1}$$

In view of the assumption of a small thickness of the layer, for the considered melt flow with a free surface it is assumed that in the layer the pressure distribution obeys the hydrostatic law, which can be written in dimensionless form as

$$\bar{p} = \frac{\delta}{\mathrm{Fr}^2}[\Psi(\bar{x}) - \bar{y}]. \tag{2}$$

In the two-phase region, the Darcy number is a function of the volume fraction of the liquid phase and is defined by the relation [13, 15]

$$\mathrm{Da} = \frac{d^2}{180L^2}\frac{\varepsilon^3}{(1-\varepsilon)^2}. \tag{3}$$

The coefficient F, which includes inertia forces, can be calculated, following [27]:

$$F = 0.13\varepsilon^{-3/2}. \tag{4}$$

The continuity equation

$$(1-\rho_s^*)\frac{\partial \varepsilon}{\partial \bar{x}} + \frac{\partial \bar{u}}{\partial \bar{x}} + \frac{\partial \bar{v}}{\partial \bar{y}} = 0. \tag{5}$$

The energy equation

$$(\rho c)^* \frac{\partial \Theta}{\partial \bar{x}} + \bar{u} \frac{\partial \Theta}{\partial \bar{x}} + \bar{v} \frac{\partial \Theta}{\partial \bar{y}} = \frac{1}{\delta^2 \operatorname{Re} \operatorname{Pr}} \frac{\partial}{\partial \bar{y}} \left(k^* \frac{\partial \Theta}{\partial \bar{y}} \right) - \frac{1}{\operatorname{Ste}} \frac{\partial \varepsilon}{\partial \bar{x}} . \tag{6}$$

For numerical realization, the last term on the right-hand side of Eq. (6) is written in the form

$$-\frac{1}{\operatorname{Ste}} \frac{\partial \varepsilon}{\partial \bar{x}} = -\frac{1}{\operatorname{Ste}} \left[\frac{\partial \varepsilon}{\partial \Theta} \frac{\partial \Theta}{\partial \bar{x}} + \frac{\partial \varepsilon}{\partial (\overline{\rho^* \Phi})} \frac{\partial (\overline{\rho^* \Phi})}{\partial \bar{x}} \right] =$$

$$= \frac{1}{\operatorname{Ste}} \left[\frac{\gamma}{(1 - \rho_s^* \kappa)} \frac{\overline{\rho^* \Phi}}{(\Theta - \Theta_p)^2} \frac{\partial \Theta}{\partial \bar{x}} + \frac{1}{(1 - \rho_s^* \kappa)} \frac{1}{(\Theta - \Theta_p)} \left(\bar{u} \frac{\partial \Theta}{\partial \bar{x}} + \bar{v} \frac{\partial \Theta}{\partial \bar{y}} \right) \right] . \tag{7}$$

The impurity conservation equation. Its form which is ordinarily used in calculations of solidification of binary alloys includes both the average impurity concentration and the impurity concentration in the liquid phase [15]. For the case of strong forced convection considered in the present work, it is found that this form of the equation leads to numerical instability. Therefore, following [9], we use the form of this equation that includes only the impurity concentration in the liquid phase:

$$[\varepsilon + \kappa \rho_s^* (1 - \varepsilon)] \frac{\partial \Phi_L}{\partial \bar{x}} + \bar{u} \frac{\partial \Phi_L}{\partial \bar{x}} + \bar{v} \frac{\partial \Phi_L}{\partial \bar{y}} = \frac{1}{\delta^2} \frac{\partial}{\partial \bar{y}} \left[\frac{\varepsilon}{\operatorname{Le} \operatorname{Re} \operatorname{Pr}} \frac{\partial \Phi_L}{\partial \bar{y}} \right] - \Phi_L (1 - \kappa) \rho_s^* \frac{\partial \varepsilon}{\partial \bar{x}} . \tag{8}$$

After determination of Φ_L per unit volume of the alloy in the two-phase region, we find

$$\overline{\rho^* \Phi} = \rho_s^* (1 - \varepsilon) \kappa \Phi_L + \varepsilon \Phi_L , \tag{9}$$

and the average mass concentration of the impurity in the two-phase region is equal to

$$\overline{\Phi} = \frac{\overline{\rho^* \Phi}}{\rho_s^* (1 - \varepsilon) + \varepsilon} . \tag{10}$$

In the present article, a linear approximation of the liquidus and solidus lines is used in the equilibrium diagram that relates the temperature and concentration of the impurity:

$$\Phi_L = (\Theta - \Theta_p)/\gamma , \quad 0 < \varepsilon < 1 ; \tag{11}$$

$$\Phi_s = \kappa \Phi_L , \quad 0 < \varepsilon < 1 . \tag{12}$$

It follows from Eqs. (9), (11), and (12) that at a certain point of the two-phase region the volume fraction of the liquid phase is defined by the relation

$$\varepsilon (\Theta, \overline{\Phi}) = \frac{\overline{\rho^* \Phi} - \rho_s^* \kappa (\Theta - \Theta_p)/\gamma}{(1 - \rho_s^* \kappa) (\Theta - \Theta_p)/\gamma} . \tag{13}$$

Equation (13) is only valid within the two-phase region, i.e., when the following inequalities are satisfied:

$$\Theta < \Theta_p , \tag{14a}$$

$$\rho_s^* \kappa (\Theta - \Theta_p)/\gamma \leq \overline{\rho^* \Phi} \leq (\Theta - \Theta_p)/\gamma . \tag{14b}$$

If at least one of the inequalities (14a) or (14b) is violated, the volume fraction of the liquid phase is defined by the following relations:

$$\varepsilon = 1 \quad \text{at} \quad \Theta > \Theta_p , \tag{15a}$$

$$\varepsilon = 1 \quad \text{at} \quad \Theta < \Theta_p \quad \text{and} \quad \overline{\rho^* \Phi} > (\Theta - \Theta_p)/\gamma , \tag{15b}$$

$$\varepsilon = 0 \quad \text{at} \quad \Theta < \Theta_p \quad \text{and} \quad \overline{\rho^* \Phi} < \rho_s^* \kappa \, (\Theta - \Theta_p)/\gamma . \tag{15c}$$

Boundary Conditions. For modeling of the continuous casting (Fig. 1), the following boundary conditions are used:

at the boundary $\bar{x} = 0$:

$$\bar{u} = \bar{u}_{in} , \quad \bar{v} = \bar{v}_{in} , \quad \Theta = \Theta_{in} , \quad \Phi_L = \Phi_{in} ; \tag{16}$$

at the boundary $\bar{y} = 0$:

$$\bar{u} = 0 , \quad \bar{v} = 0 , \quad k^* \frac{\partial \Theta}{\partial \bar{y}} = \frac{q h_\infty}{(T_{in} - T_c) \, k_L} ; \tag{17}$$

on the free surface $\bar{y} = \psi$:

$$\frac{\partial \bar{u}}{\partial \bar{y}} = 0 , \quad \frac{\partial \Theta}{\partial \bar{y}} = 0 , \quad \frac{\partial \Phi_L}{\partial \bar{y}} = 0 , \quad \frac{d\Psi}{d\bar{x}} (\bar{u} + \bar{U}) = \bar{v} . \tag{18}$$

For numerical realization, the last of boundary conditions (18) is replaced by the equivalent condition of the mass-flow-rate conservation in the cross section:

$$\int_0^{\Psi(\bar{x})} \left\{ [\varepsilon + (1 - \varepsilon) \rho_s^*] + \bar{u} \right\} d\bar{y} = \rho_s^* . \tag{19}$$

Equation (19) is obtained by integration of continuity equation (5) between 0 and h with account of the latter equation at boundary conditions (18). When Eq. (19) was obtained, it was assumed that on the free surface the entire alloy is in the liquid state. The case where on the free surface the alloy is in the two-phase state is discussed in what follows.

Modification of the Model where the Two-Phase Region Reaches the Free Surface. Impurity conservation equation (8) requires special consideration for the case where on the free surface the alloy is transformed into the two-phase state (the distance from the beginning of the casting table to the point at which this transformation occurs is designated by $\bar{X}^*$). First, Eq. (8) is rewritten in the form

$$\frac{\partial}{\partial \bar{x}} [\bar{U} \overline{\rho^* \Phi}] + \frac{\partial}{\partial \bar{x}} [\bar{u} \, \Phi_L] + \frac{\partial}{\partial \bar{y}} [\bar{v} \, \Phi_L] = \frac{1}{\delta^2} \frac{\partial}{\partial \bar{y}} \left[\frac{\varepsilon}{\mathrm{Le \, Re \, Pr}} \frac{\partial \Phi_L}{\partial \bar{y}} \right] . \tag{20}$$

The physical meaning of Eq. (8) consists in the fact that the mass of the impurity per unit volume can be changed both by the relative motion of the liquid phase and by diffusion of the impurity in the liquid phase.

We consider the impurity flow rate through the cross section of the strip. It is evident that the amount of impurity that passes through the cross section of the strip in the direction of the $\bar{x}$ axis should be the same in any cross section. Integrating Eq. (20) from 0 to Ψ and using Eq. (19) and boundary conditions (17) and (18), we arrive at the following relation:

$$\frac{\partial}{\partial \bar{x}} \int_0^{\Psi(\bar{x})} [\bar{U}\,\overline{\rho^* \Phi} + \bar{u}\,\Phi_L]\, d\bar{y} = -\,\bar{U}\,\frac{d\Psi}{d\bar{x}}\,\Phi_L\,(1-\varepsilon)\,(1-\rho_s^* \kappa)\,|_{\bar{y}=\Psi(\bar{x})}\,. \tag{21}$$

In its physical meaning, the integral on the left-hand side of Eq. (21) determines the impurity mass flow rate through the cross section whose distance from the beginning of the casting table is determined by the coordinate $\bar{x}$. This mass flow rate should be the same at any coordinate $\bar{x}$. This condition is evidently satisfied until $\varepsilon = 1$ at $\bar{y} = \Psi(\bar{x})$, since at $\varepsilon = 0$, the right-hand side of Eq. (21) becomes zero. This condition is violated when $\varepsilon < 1$, i.e., when on the free surface the alloy is transformed into the two-phase state. According to Eq. (9), at a specified temperature, the equilibrium concentration of the impurity is higher in the liquid phase than the average concentration in the two-phase region. When on the free surface the alloy is transformed into the two-phase state, it follows from Eq. (21) that the amount of impurity that is transported to the free surface exceeds its amount that should be on the free surface in accordance with the equilibrium relations. This result implies a conflict between the equilibrium relations and the conservation laws that appears when one tries to use Eq. (8) at $\bar{x} > \bar{X}^*$. Therefore, if $\bar{x} > \bar{X}^*$, the mathematical model described by Eqs. (1), (5), (6), and (8) becomes incorrect, and it is necessary to use an alternative mathematical model.

At $\bar{x} > \bar{X}^*$ the liquid-phase flow relative to the solidified material is small and can be neglected. This results in the following form of the momentum equation:

$$\bar{u} = 0\,. \tag{22}$$

Thereby we assume the absence of relative motion in the direction of the $\bar{x}$ axis. Therefore, motion that is caused by shrinkage of the alloy in the two-phase region is the only motion that takes place in a layer of the material. Consequently, the motion in the direction of the $\bar{y}$ axis (which has the negative velocity $\bar{v}$) is the only relative motion in the strip. Since it is assumed that both in the layer of the alloy and on the free surface, porosity is not formed, this motion of the layer inevitably causes deformation of the solid phase in the two-phase region and induces motion of both solid and liquid phases. Now, in the averaging volume, these phases move as a unit. These assumptions lead to the following form of the continuity, energy, and impurity conservation equations:

$$(1-\rho_s^*)\,\frac{\partial \varepsilon}{\partial \bar{x}} + [\varepsilon + \rho_s^*\,(1-\varepsilon)]\,\frac{\partial \bar{v}}{\partial \bar{y}} + \bar{v}\,(1-\rho_s^*)\,\frac{\partial \varepsilon}{\partial \bar{y}} = 0\,, \tag{23}$$

$$(\rho c)^*\,\frac{\partial \Theta}{\partial \bar{x}} + (\rho c)^*\,\bar{v}\,\frac{\partial \Theta}{\partial \bar{y}} = \frac{1}{\delta^2 \mathrm{Re}\,\mathrm{Pr}}\,\frac{\partial}{\partial \bar{y}}\left(k^*\,\frac{\partial \Theta}{\partial \bar{y}}\right) - \frac{1}{\mathrm{Ste}}\,\frac{\partial \varepsilon}{\partial \bar{x}}\,. \tag{24}$$

In order to obtain Eq. (24), we used an additional assumption that the velocity of vertical motion $\bar{v}$ varies slowly relative to the coordinate $\bar{y}$.

For numerical realization, the last term in Eq. (24) should be replaced with account of Eq. (7).

Finally, at $\bar{x} > \bar{X}^*$, Eq. (8) is replaced by the following equation:

$$\frac{\partial}{\partial \bar{x}}\,[\,\overline{\rho^* \Phi}\,] + \frac{\partial}{\partial \bar{y}}\,[\bar{v}\,\overline{\rho^* \Phi}\,] = 0\,. \tag{25}$$

For Eqs. (23)-(25) the boundary conditions are as follows:

at the boundary $\bar{y} = 0$

$$\bar{v} = 0\,,\quad k^*\,\frac{\partial \Theta}{\partial \bar{y}} = \frac{q h_\infty}{(T_{in} - T_c)\,k_L}\,; \tag{26}$$

on the free surface $\bar{y} = \Psi$:

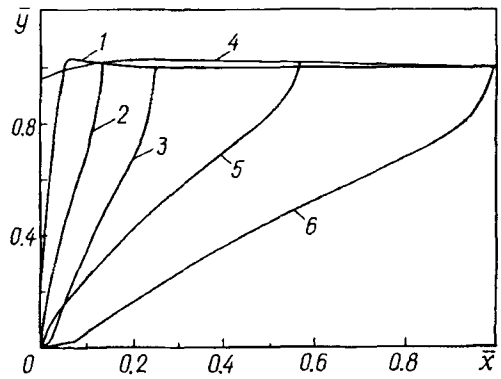

Fig. 2. Locations of free surface (1, 4), liquidus (2, 5), and solidus (3, 6) at rates of drawing of 0.1 m/sec (1-3) and 0.4 m/sec (4-6).

$$\frac{\partial \Theta}{\partial \bar{y}} = 0\,, \quad \bar{\Phi} = \text{const} \tag{27}$$

plus the integral condition specified by (19). Equation (19) is used with account of the assumption that the horizontal component $\bar{u}$ of the velocity of relative motion becomes zero at $\bar{x} > \bar{X}^*$.

The boundary condition used for Eq. (25) is specified as the second one in (27) and needs special discussion. Equation (25) is a transfer equation and requires only one boundary condition for its solution. Since the velocity of vertical motion $\bar{v}$ is negative at $\bar{x} > \bar{X}^*$, it is necessary to indicate the boundary condition on the free surface. Here, the impurity mass per unit volume $\overline{\rho C}$ that includes both liquid and solid phases increases as solidification continues. This increase is caused by volume shrinkage of the alloy in the two-phase region and, as a consequence, by increasing the average density of the material in the averaging volume. On the other hand, the average mass fraction $\bar{C}$ of the impurity remains constant. This can be attributed to the assumption that at $\bar{x} > \bar{X}^*$, a mixture of liquid and solid phases moves as a unit in the averaging volume. Thus, at $\bar{x} > \bar{X}^*$ the boundary condition that is used for the impurity conservation equation has the physical meaning that the impurity fraction $\bar{C}$ ($\bar{\Phi}$ in the dimensionless form) remains unchanged after the alloy was transformed into the two-phase state on the free surface.

Analysis of Numerical Results. Practical calculations were carried out for the binary system NH_4Cl-H_2O, containing 0.1% of H_2O (water is an impurity). In the future, it is planned to conduct an experimental study on a model setup. Ammonium chloride was chosen as a binding material because it has a low melting temperature, which makes creation of the experimental setup easier. It should be noted that since the growth of dendrites that accompanies solidification of the system NH_4Cl-H_2O is similar to this growth that accompanies solidification of metal alloys, this system was used repeatedly for simulation of solidification of metals [13, 15]. In calculations, the following thermophysical properties of the material and process parameters were used: $L = 2$ m; $h_\infty = 0.0014$ m; $T_{in} = 600$ K; $T_p = 632.42$ K; $T_c = 273.15$ K; $C_{in} = 0.1\%$; $C_E = 0.803\%$; $\rho_L = 1033$ kg/m^3; $\rho_s = 1078$ kg/m^3; $k_L = 0.468$ W/m·K; $k_s = 0.393$ W/m·K; $c_L = 3249$ J/(kg·K); $c_s = 1870$ J/(kg·K); $\Delta h = 3.138 \cdot 10^5$ J/kg; $q = 3.2 \cdot 10^5$ W/m^2; $\nu_L = 1.206 \cdot 10^{-6}$ m^2/sec; $d = 1 \cdot 10^{-4}$ m; $D_L = 4.8 \cdot 10^{-9}$ m^2/sec; $\Gamma = -467$ K; $\kappa = 0.3$. The calculations were carried out on a Silicon Graphics XL R10 000 supercomputer in a finite-difference network with $5 \cdot 10^3$ points in the $\bar{x}$ axis and $5 \cdot 10^3$ points in the $\bar{y}$ axis.

In Fig. 2, one can see positions of the free surface, liquidus, and solidus at various rates of drawing of the strip. It can be seen that at rates of drawing of up to 0.4 m/sec, the shape of the free surface is almost horizontal. Since the density of the heat flux that is transferred from the strip–casting table contact surface remains constant, an increase in the rate of drawing leads to an increase in both the width of the two-phase region and its dimension in the direction of the $\bar{x}$ axis. The curves in Fig. 2 were calculated with account of diffusion of the impurity in the liquid phase.

Figure 3 shows the distribution of the average concentrations of the impurity at the beginning of the casting table (at $\bar{x} = 0$) and after cessation of solidification (at $\bar{x} = 1$) at different rates of drawing of the strip. These distributions were calculated with account of diffusion of the impurity in the liquid phase and neglecting it.

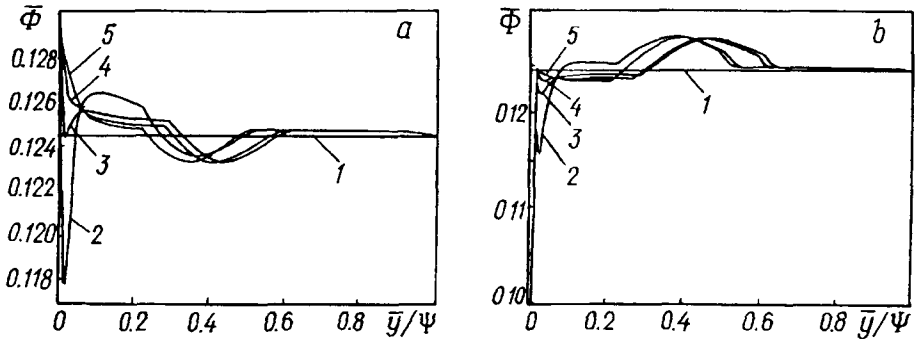

Fig. 3. Distributions of average impurity concentrations at the beginning of the casting table (1) and after completion of solidification at rates of drawing of 0.1 (2), 0.2 (3), 0.3 (4), and 0.4 m/sec (5), neglecting (a) and including (b) diffusion of impurity in the liquid phase.

Comparison of Fig. 3a and b shows that the effect of diffusion is especially pronounced at the surface of the casting table. Here diffusion of the impurity in the liquid phase brings about a formation of the diffusion boundary layer that is characterized by a low content of the impurity. This formation can easily be explained in view of the fact that the lower boundary of the strip is simulated as a wall impermeable for the impurity. Heat is transferred simultaneously from this boundary, which results in a sharp gradient of the liquid fraction. Since in solidification the impurity is displaced from solidifying dendrites into the interdendrite liquid, the gradient of the volume fraction of the liquid phase leads to a sharp concentration gradient of the impurity in the liquid phase (as the distance to the lower boundary of the strip decreases, the smaller amount of the liquid phase remains and the higher amount of the impurity is displaced into the liquid phase). Thus, solidification of the alloy at the lower boundary of the strip is characterized by the following: as the distance to the casting table decreases, the impurity concentration in the liquid phase increases. This gives rise to high-intensity diffusion transfer of the impurity in the averaging volume (it includes both the liquid and the solid phase) at the lower boundary.

On the contrary, the calculations that neglected diffusion transfer of the impurity (Fig. 3a) show that the impurity concentration increases at the surface of the casting table. This is caused by high-intensity transfer of the impurity to the surface of the casting table by the interdendrite liquid flow that compensates for solidification shrinkage of the material (the so-called inverse microliquation).

Thus, in the real situation (Fig. 3b), at the surface of the casting table two competing processes have an important effect on the impurity redistribution, namely, diffusion of the impurity in the liquid phase, which decreases the amount of the impurity at the boundary, and an interdendrite liquid flow, which increases the impurity concentration at the boundary. It should be noted that the effect of diffusion is important only in the narrow boundary layer at the surface of the casting table, outside which it rapidly weakens. Therefore, interaction of these two factors results in a concentration profile that has a local maximum at the surface of the casting table.

As the distance from the casting table increases, forced convection and interdendrite filtration that compensates for shrinkage become controlling factors. The latter leads to downward transport of the impurity, but its effect is proportional to the solidification rate, i.e., it rapidly becomes weaker as the distance from the surface of the casting table increases. On the contrary, transfer of the impurity by forced convection caused by increasing the height of the free surface results in upward transport of the impurity. It should be noted that the convection rate increases as the distance to the free surface decreases. Therefore, the local maximum of the impurity concentration that is located near the casting table (this maximum is generated by interdendrite filtration) is replaced by a local minimum that is caused by transfer of the impurity by forced convection from the lower part of the strip to its central part. Since the forced-convection intensity correlates with the rate of change in the height of the free surface, the depth of this minimum is maximal at $U = 0.1$ m (a substantial change in the height of the free surface) and minimal at $U = 0.4$ m/sec (the free surface is almost horizontal). Finally, the local maximum of the impurity concentration observed in the central part of the strip is caused by transport of the impurity by forced convection.

Conclusions. It has been found that although the effect of diffusion transfer of the impurity is maximal at the surface of the casting table, calculations that are performed with neglect of diffusion for the system NH_4Cl-H_2O give a qualitatively incorrect impurity distribution over the thickness of the strip. However, it should be noted that for binary metal alloys, the diffusion coefficient of the alloying component is ordinarily much lower than it is in the system NH_4Cl-H_2O; therefore, it can be expected that for metal alloys diffusion will result in a more local surface effect. Concentration profiles that were calculated with account of diffusion have a local maximum near the surface of the casting table. The local maximum is subsequently replaced by a local minimum and again by a local maximum in the center of the strip. This form of concentration distribution of the impurity can be explained by competing interactions of various mechanisms of impurity transfer, namely, diffusion transfer, impurity transfer by interdendrite filtration that compensates for solidification shrinkage, and transfer of the impurity by forced convection.

The author is grateful to the A. Humboldt Foundation and the Technical University of Vienna for support of this study.

NOTATION

c, specific heat, J/(kg·K); c_L, c_s, mass fractions of impurity in liquid and solid phases; $\overline{C}$, average mass fraction of impurity in the two-phase region, $\overline{\rho C}/[\rho_s(1-\varepsilon)+\rho_L\varepsilon]$; C_E, mass fraction of impurity in the eutectic; d, average diameter of the base of primary branches of dendrites, m; D_L, diffusion coefficient of impurity in interdendrite liquid, m^2/sec; Da, Darcy number, K/L^2; Fr, Froude number, $U/\sqrt{gL}$; h, height of the free surface, m; h_∞, height of the free surface at the end of the casting table (after completion of solidification), m; k, thermal conductivity, W/(m·K); k^*, ratio of thermal conductivity, $[\varepsilon k_L+(1-\varepsilon)k_s]/k_L$; K, permeability, m^2; L, length of the casting table, m; Le, Lewis number, α_L/D_L; p, pressure, Pa; $\overline{p}$, dimensionless pressure, $p/(\rho_L U^2)$; Pr, Prandtl number, ν_L/α_L; q, density of the heat flux transferred from the surface of the casting table, W/m^2; Re, Reynolds number, UL/ν_L; Ste, Stefan number, $c_L(T_{in}-T_c)/\Delta h$; T, temperature, K; T_p, melting temperature of ammonium chloride, K; T_c, temperature of coolant, K; v, vertical velocity component, m/sec; $\overline{v}$, dimensionless vertical velocity component, $v/(U\delta)$; u, horizontal component of relative velocity, m/sec; $\overline{u}$, dimensionless horizontal component of relative velocity, u/U; U, rate of drawing of the strip, m/sec; $\overline{U}$, dimensionless rate of drawing of the strip, $U/\overline{U}=1$; x, horizontal coordinate, m; $\overline{x}$, dimensionless horizontal coordinate, x/L; X^*, distance from the beginning of the casting table, when the alloy of the free surface is transformed into a two-phase state, m; $\overline{X^*}$, dimensionless distance from the beginning of the casting table, when alloy on the free surface is transformed into a two-phase state, X^*/L; y, vertical coordinate, m; $\overline{y}$, dimensionless vertical coordinate, y/h_∞; α, thermal diffusivity, $k/(\rho c)$, m^2/sec; δ, ratio of the thickness of the strip to the length of the casting table, h_∞/L; Δh, specific heat of melting, J/kg; ε, volume fraction of the liquid phase; Φ_L, dimensionless impurity concentration in the liquid phase, C_L/C_E; Φ_s, dimensionless impurity concentration in the solid phase, C_s/C_E; $\overline{\Phi}$, dimensionless average impurity concentration, $\overline{C}/C_E$; γ, dimensionless slope of the liquidus line, $\Gamma C_E/(T_{in}-T_c)$; Γ, slope of the liquidus line, K; κ, coefficient of equilibrium impurity distribution between solid and liquid phases in the two-phase region, C_s/C_L; μ_L, dynamic viscosity of the liquid phase, kg/(m·sec); ν_L, kinematic viscosity of the liquid phase, m^2/sec; Θ, dimensionless temperature, $(T-T_c)/(T_{In}-T_c)$; ρ, density, kg/m^3; ρ_s^*, ratio of densities of solid and liquid phases, ρ_s/ρ_L; $(\rho c)^*$, ratio of heat-accumulating capacities, $[\varepsilon\rho_L c_L+(1-\varepsilon)\rho_s c_s]/\rho_L c_L$; $\overline{\rho C}$, mass of impurity per unit volume in the two-phase region. $\rho_s(1-\varepsilon C_s+\rho_L\varepsilon C_L$, kg/m^3; $(\rho^*\Phi)$, dimensionless mass of impurity per unit volume in the two-phase region, $\overline{\rho C}/\rho_L C_L$; Ψ, dimensionless thickness of the strip, h/h_∞. Subscripts: in, refers to $x=0$; L, refers to liquid phase; p, pure ammonium chloride; s, solid phase.

REFERENCES

1. M. Shiomi, K. Mori, and K. Osakada, Proc. Conf. "Modeling of Casting, Welding, and Advanced Solidification Processes. VII" (1995), pp. 793-800.

2. C.-M. Reihle, H. Fredriksson, and S. Ostlund, Proc. Conf. "Modeling of Casting, Welding, and Advanced Solidification Processes. VII" (1995), pp. 812-824.
3. P. J. Bradbury and J. D. Hunt, Proc. Conf. "Modeling, of Casting, Welding, and Advanced Solidification Processes. VII" (1995), pp. 739-746.
4. W. D. Bennon and F. P. Incropera, Int. J. Heat Mass Transfer, **30**, 2116-2170 (1967).
5. P. J. Presscott, F. P. Incropera, and W. D. Bennon, Int. J. Heat Mass Transfer, **34**, 2351-2359 (1990).
6. J. Ni and F. P. Incropera, Int. J. Heat Mass Transfer, **38**, 1271-1284 (1995).
7. J. Ni and F. P. Incropera, Int. J. Heat Mass Transfer, **38**, 1285-1296 (1995).
8. S. Ganesan and D. R. Poirier, Metallurg. Trans., **21B**, 173-181 (1990).
9. D. B. Poirier, P. J. Nandapurkar, and S. Ganesan, Metallurg Trans., **22B**, 889-900 (1991).
10. J. Ni and C. Beckermann, Metallurg. Trans., **228**, 349-361 (1991).
11. R. Viskanta, JSME Int. J. Series II, **33**, 409-423 (1990).
12. A. V. Kuznetsov and K. Vafai, Int. J. Heat Mass Transfer, **38**, 2557-2567 (1995).
13. W. D. Bennon and F. P. Incropera, Int. J. Heat Mass Transfer, **30**, 2171-2187 (1987).
14. V. R. Voller and C. Prakash, Int. J. Heat Mass Transfer, **30**, 1709-1719 (1997).
15. C. Beckermann and R. Viskanta, Phys.-Chem. Hydrodynamics, **10**, 195-213 (1988).
16. W. D. Bennon and F. P. Incropera, Numer. Heat Transfer, **13**, 277-296 (1988).
17. A. H. H. Engel and F. P. Incropera, Wärme- und Stoffübertragung., **24**, 279-288 (1989).
18. V. R. Voller, A. D. Brent, and C. Prakash, Int. J. Heat Mass Transfer, **32**, 1719-1731 (1989).
19. C. Prakash and V. Voller, Numer. Heat Transfer B., **15**, 171-189 (1989).
20. D. G. Neilson, F. P. Incropera, and W. D. Bennon, Int. J. Heat Mass Transfer, **33**, 367-380 (1990).
21. S. D. Felicelli, J. C. Heinrich, and D. R. Poirier, Metallurg. Trans. B., **22**, 847-859 (1991).
22. H. Yoo and R. Viskanta, Int. J. Heat Mass Transfer, **35**, 2335-2346 (1992).
23. S. D. Felicelli, J. C. Heinrich, and D. R. Poirier, Numer. Heat Transfer B, **23**, 461-481 (1993).
24. S. L. Lee and R. Y. Tzong, Int. J. Heat Mass Transfer, **38**, 1237-1247 (1995).
25. M. C. Schneider and C. Beckermann, Int. J. Heat Mass Transfer, **38**, 3457-3473 (1995).
26. W. F. A. Böhmer, M. C. Schneider, C. Beckermann, and P. R. Sahm, Proc. Conf. "Modeling of Casting, Welding, and Advanced Solidification Processes. VII" (1995), pp. 617-624.
27. G. S. Beavers and E. M. Sparrow, J. Appl. Mech., **36**, 711-714 (1969).